

Satellite gravity anomalies and crustal features of the Central Indian Ocean Basin

D. Gopala Rao^{1,*}, K. S. Krishna¹, Yu. P. Neprochnov² and B. N. Grinko²

¹National Institute of Oceanography, Dona Paula, Goa 403 004, India

²P.P. Shirshov Institute of Oceanology, 36 Nakhimovsky Prospect, Moscow 117 851, Russia

Satellite free-air gravity anomaly contour map at 5 mGal interval, seismic reflection and bathymetric data lead to the identification of deformed crustal structure of the Central Indian Ocean Basin. Twenty-three NE-SW trending deformed crustal features have been identified between 5°S to 4°N and 77° to 89°E. Pattern of deformation varies with large relief anticlines in the west, numerous long wavelength anticlinal basement rises in the middle of the basin, and zones of high-angle reverse faults and low-amplitude broad basement rises dominated with reverse faults in the east. Their disposition and deformation pattern record excess folding and shortening in the east of the basin. A chain of near circular free-air anomalies due to volcanic constructs that trend in arcuate shape from north to south parallel to 82.5°E are noted as southern continuity of the 85°E Ridge, which terminates at the Afanasy Nikitin seamount. Change in rheology of the crustal rocks and deformation in the east appear to result due to high heat-flow in the middle of the basin and intense seismicity of the eastern part of the basin. The present plate boundary forces contribute to the change in physical state and architecture of deformation of crust and result in vast area undergoing NNW-SSE to NW-SE compression.

THE oceanic crust between 5°N to 10°S and 77 to 89°E in the Central Indian Ocean Basin (CIOB) was evolved by the spreading systems, India–Antarctica and Wharton Ridges, during the mid-Cretaceous to late Paleocene (Figure 1). The Afanasy Nikitin seamount (ANS), a major crustal feature, lies in the middle of the CIOB. Seismic reflection investigations at selected places in the CIOB^{1–6} have imaged the sediment structure, morphology of the basement and some of the deformation features (long-wavelength anticlinal basement rises and high-angle reverse faults). The Ocean Drilling Program (ODP) Leg 116 drilling and other results on an upthrust deformed block near the equator have indicated deformation of oceanic crust initiated at late Miocene (7.5–8.0 Ma)^{7–10}. The 86°E FZ acted as plate boundary between India–Antarctica Ridge and Wharton Ridge till the end of middle Eocene, 42 Ma^{11,12}. Seismic stratigraphic analysis has revealed that four seismic

sequences, as thick as 3 km, overlie the mid-Cretaceous oceanic basement. They are separated by three structural unconformities (upper Miocene, lower Pliocene and upper Pleistocene)^{2,10,11}. Long-term diffuse deformation of the CIOB has been suggested¹³. Reverse faults propagate downwards up to 10 km in the crust and upper mantle¹⁴. Spacing of faults is proportional to depth of localization instabilities¹⁵, which depends on the effective stress component¹⁶. However, extent and kinematics of deformation are not clearly known. Efforts are in progress to understand them. The present study is aimed to map the deformed crustal blocks to limit the area of deformation, note the architecture of the deformed crustal blocks and infer kinematics of deformation.

Geophysical investigations

Free-air gravity anomaly map at 5 mGal contour interval (Figure 2) was prepared for the CIOB area between 5°N to 10°S and 76° to 90°E from Geosat and ERS-1 satellite altimetry data¹⁷. Seismic reflection, gravity and bathymetric data collected in three polygons (S22-I to III) and along four regional profiles, 4, 7, 8 and 9 during the 22nd cruise of R/V *Professor Shtokman* in 1989 and published results from the seismics (Figure 1) were also gathered to consider as ground truth for identified crustal structure from the anomalies. Bathymetry maps at varied contour intervals of the polygons and also the polygon M31-V (from the data collected on-board R/V *Akademik Mstislav Keldysh* during 1977) prepared by Evsykov⁸ are presented in Figure 3 *a–d*. Free-air gravity anomalies along two regional profiles AS 10-03 and 10-05, collected during the R/V *A.A. Sidorenko* cruise are presented in Figure 4 along with the satellite gravity anomalies along the profiles for comparison. Single-channel seismic records of profiles 4 and 7 are given in Figure 5 *a* and *b* along with interpreted line diagrams and selected parts of the deformed blocks in Figure 6 *a–d*. The deformed blocks that are identified from the gravity in correlation with seismic reflection and bathymetric results are presented in Figure 7, which illustrates their disposition and architecture. The range and amplitude of anomalies, geometry (width, relief and fault pattern), thickness of overlying sediments and inferred time of deformation of the each crustal block that is identified from the studies along with the seismicity,

*For correspondence. (e-mail: gopalrao@darya.nio.org)

heat flow and fault pattern of the identified deformed crust blocks are given in Table 1.

Results

Bathymetry

The seafloor topography in S22-I area (Figure 3 *a*) varies from 4308 to 4950 m water depth and depicts three distinct geomorphic features: highs in the northeast and southwest and a plain with small undulations extending from northwest to southeast and highs in the northeast and southwest. In the plain, water depth varies from 4770 to 4827 m, with an average of 4800 m. The highs rise by 550 and 490 m respectively, from the surrounding seafloor at 4800 m depth. Several E-W trending small-scale lineations 7 to 22 km long and 40 to 150 m wide are superposed on these highs.

The seafloor topography in S22-II area (Figure 3 *b*) depicts two oval-shaped highs at the centre and several small-scale rises in the southwest. The high in the south trends NE-SW and is 105 km long and 70 km wide, with 725 m relief from surrounding flat-bottom seafloor at 4650 m

depth. It has uniform gradient of rise in three sides, whereas in the southeast the gradient is relatively steep. The high in the north trends nearly E-W with axes of 95 and 120 km, composed of several small-scale 100 to 300 m rises and differs in orientation and morphological expression from the high in the south, indicating that both were evolved in different geological processes.

The seafloor topography of S22-III area (Figure 3 *c*) varies from 4380 to 4415 m water depth and is generally smooth and deepens towards south. It also depicts low relief topographic highs trending NE-SW. The bathymetry in the M31-V area (Figure 3 *d*) west of the ANS at 4°S and 82°30'E varies from 4465 to 5200 m and outlines detailed seafloor morphology of the outcropped deformed block of oval shape. It trends NE-SW with axes of about 90 and 185 km and rises by about 530 m from the surrounding seafloor of 5000 m. E-W trending minor topographic lineations are superposed on the high. These observations clearly record NE-SW trending high relief long wavelength seafloor topographic features of some of the crustal blocks in the CIOB.

Satellite gravity data

The free-air gravity anomaly map of the area (Figure 2) between 5°N to 10°S and 76° to 90°E shows several distinct anomaly closures either elongated NE-SW or circular in the basin. The NE-SW trending anomalies are numbered 1 to 23 and occur in the middle of the CIOB and their boundaries are marked. Besides, circular to oval

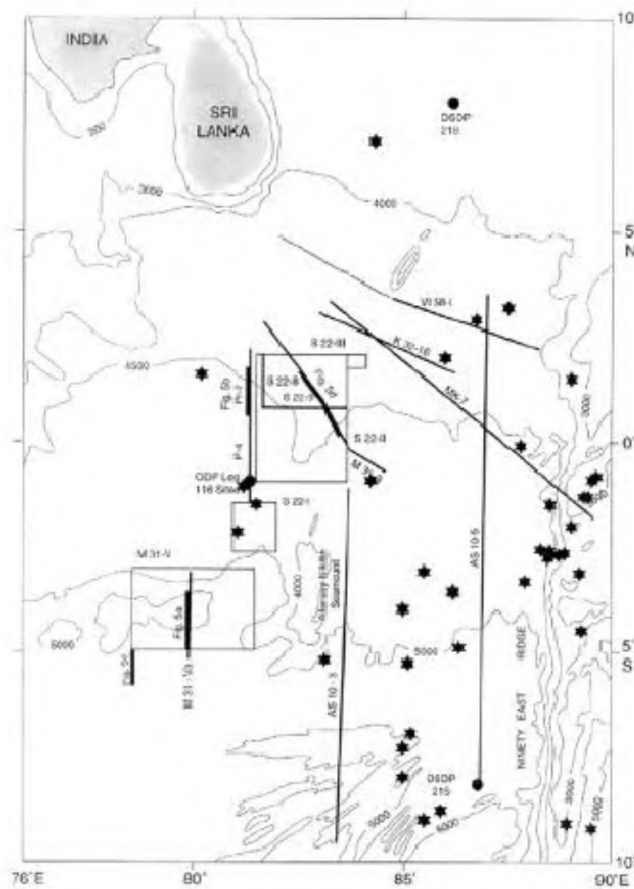


Figure 1. Location map showing bathymetry (thin line)²⁸, seismic profiles (thickness; data details given in Table 1), areas of detailed investigations squares, locations of earthquake epicentres (stars)²⁹⁻³¹ and location of the ODP and DSDP drill sites solid circles.

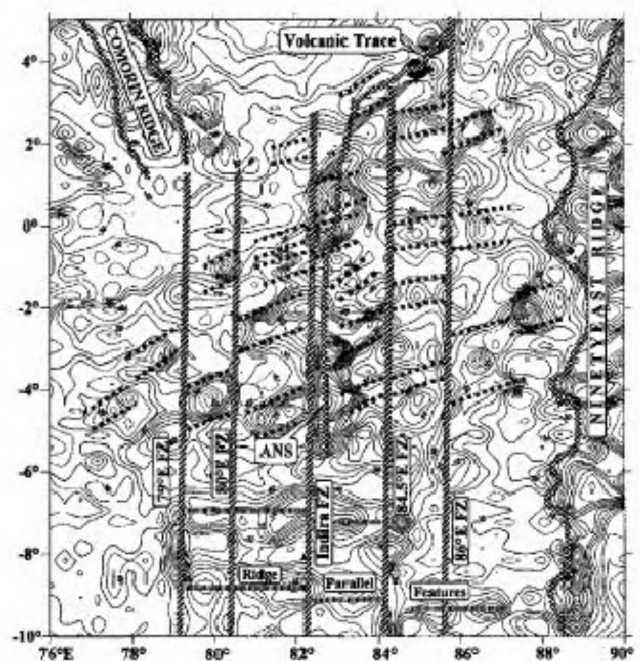


Figure 2. Satellite free-air gravity anomaly map (Geosat and ERS-1 altimetry data by Sandwell and Smith¹⁷).

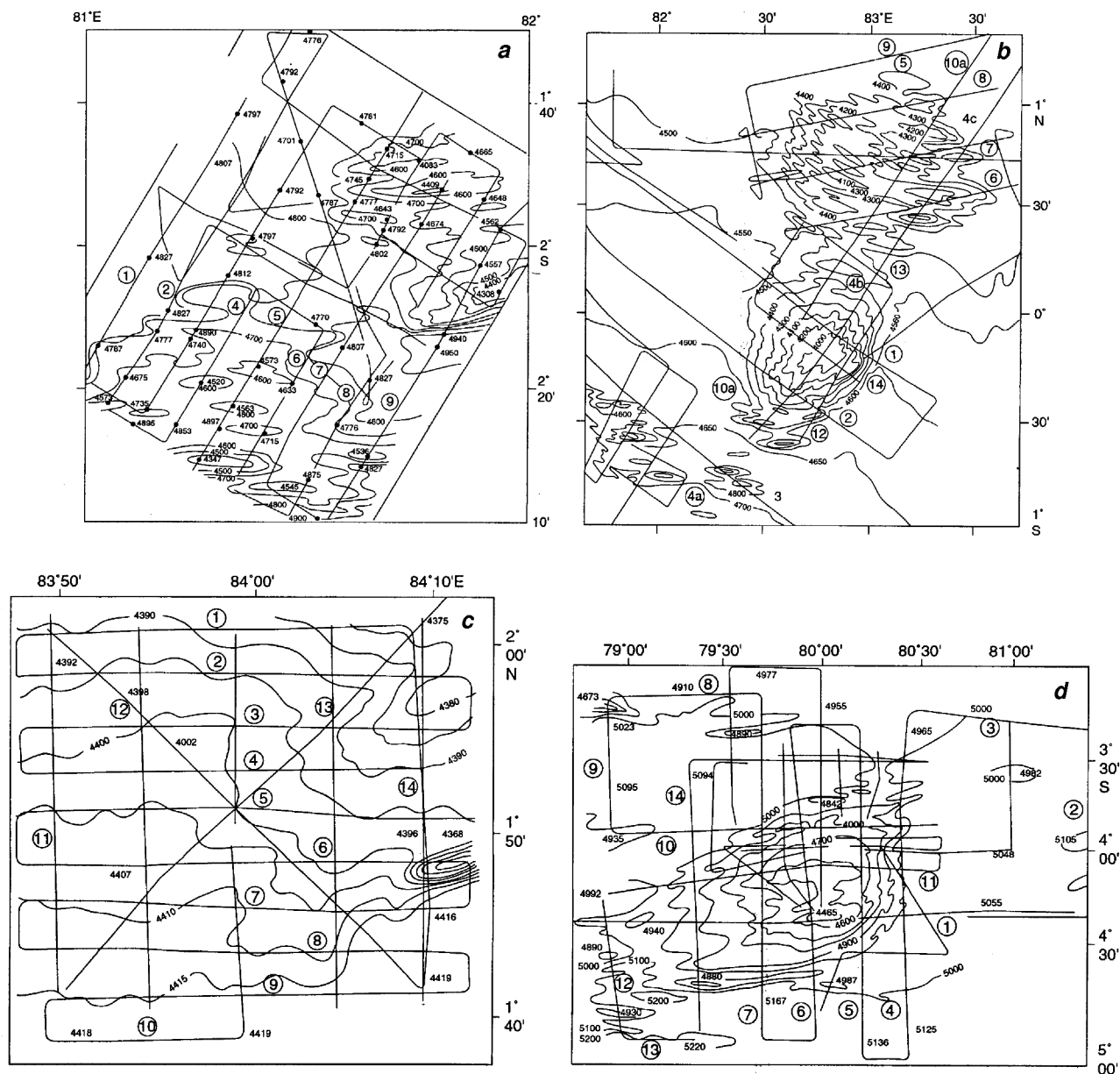


Figure 3 a-d. Seafloor topographic maps of varied (10 to 100 m) contour intervals, covering S22-I, II, III and M31-V respectively. Depths in metres are also given as spot values.

shaped anomalies in the east (parallel to 90°E), south and northwest also occur. They are also noted along with their boundaries (Figure 2). The anomaly amplitudes vary from 15 to 45 mGal. Comparison of satellite and ship-borne free-air gravity anomalies on profiles AS 10-3 and 10-5 (Figure 4) reveals that both satellite and ship-borne anomalies are fairly in good agreement with some deviations of about 3–4 mGal, which is within the accuracy limits of the satellite free-air gravity data¹⁷. Further, a double-peaked NE-SW trending anomaly around 0°N and $82^{\circ}30'\text{E}$ is noted, which corresponds to the one observed in ship-borne free-air gravity anomalies of the S22-II area¹⁸. Therefore, the satellite positive amplitude free-air gravity anomalies

of the basin are reliable to identify the long-wavelength deformed crustal blocks. The boundaries have been marked and they show NE-SW trend as well as circular/oval-shaped anomalies. Their NE-SW trending anomalies abut mostly against N-S trending fracture zones. They are numbered 1 to 23 and are shown in Figure 7. The near-circular anomaly amplitudes in the middle of the basin (around 4°S and 82.5°E) are relatively high, up to 70 mGal associated with the prominent physiography features of the ANS and mark not only differing trends but also anomalous crustal features that adjoin each other and form a chain between 5°S and 3°N parallel to 82.5°E . Further north, they veer towards northeast and appear to continue

beyond the study area. Some of the anomaly closures in the east of the ANS culminate against anomalies of the seamount. Even though the widths, disposition and amplitudes of the NE-SW trending anomalies vary, they are relatively more closely spaced around the seamount. Free-air gravity anomalies south of 6°S are mostly elongated and their axial highs mark E-W trends and are parallel to spreading ridge trends. A series of circular anomaly closures also occur in the northwest of 2°N, which are also juxtaposed to each other. They appear to continue northwest beyond the study area and are associated with the Comorin Ridge-related structures. A series of high-amplitude near-circular to elongated anomaly closures adjoining each other extend longitudinally between 88° and 90°E. The pattern and disposition of the circular anomalies are quite distinct from the elongated NE-SW trending anomalies of the CIOB and the E-W trending anomalies in the south. Thus the gravity anomalies clearly depict loci of the deformed crust blocks and other non-deformed crustal features of the area. The heat flow is above normal, 50 mW/m² in the area^{19,20} and the seismicity is compressional, mostly in northwest-south east²¹.

Seismic reflection

The seismic reflection records of profiles 4 and 7 (Figure 5 *a* and *b*) and published profiles 8 and 9 reveal seismic sequences O, A, AA and B (from bottom to top) within sediments, 2.0 to 2.6 s (TWT) thick. Varied types of deformation features of the basement are noted and they mostly upthrust against high-angle faults of the deformed anticline structures (Figure 6 *a-d*). The deformed features are regular in pattern and limited between 4°N and 5°S. The results and their seismic reflection pattern are noted in Table 1. The seismic sequence stratigraphic boundary Oligocene (O) and structural unconformities of upper Miocene (A), lower Pliocene (AA) and upper Pleistocene (B) and seafloor are correlated to ODP Leg 116 results^{10,11,22}.

Profile 4 (Figure 5 *a*) clearly depicts the deformed basement and the overlying reflectors of the sequences against high-angle faults overlain by parallel reflectors of the top sequence in the south. They are identified as the two deformed crustal blocks that are noted (Figure 3) with squares and numbered as 5 and 6 (Figure 7), and are between 100 and 180 km and 190 and 280 km distances respectively, on profile 4 (Figure 5 *a*). Widely spaced near-vertical faults and less deformed basement have also been noted towards north on the profile. An unusual U-shaped major seafloor depression of about 110 m deep and 18 km wide occurs on the southern flank of the deformed block 5 between 210 and 228 km distance (Figure 5 *a*). Beneath it, the basement and sediment reflectors as well show syn-genetic down-faulting associated with anticline denoting antithetic movement of top of the basement of the deformed block 5.

The seismic images of profile 7 (Figure 5 *b*) show stratified sediments of the deformed basement consisting of a series of rises 0.3 to 1.7 s relief and 4 to 8 km wide in the north. At the northern end of profile 8 (ref. 23), such images of the basement are noted beneath 2.6 s thick sediments comprising several rises, about 0.2 s relief and, noted as deformed block 23. While on profile 9 (ref. 23), the reflectors of the basement block 10 and overlying sediments depict deformation and about 0.7 s relief at the basement level near the Indira FZ in the west. It has also been noted by earlier workers²³ on profiles M31-3-BB', S22-C and S33-11.

The seismic reflectors of the basement and sediments on profile M31-3 (Figure 6 *d*) show broad anticlinal structure between 0° and 1.5°N consisting of double-peaked rises/highs, which are noted as 10 and 11 deformed blocks. The rises and overlying deformed sediments are associated with distinct free-air gravity signatures trending NE-SW in the south and near-circular in the north (Figure 2). They are viewed as independent deformed crustal blocks 10 and 11. The high in the south depicts equal relief of

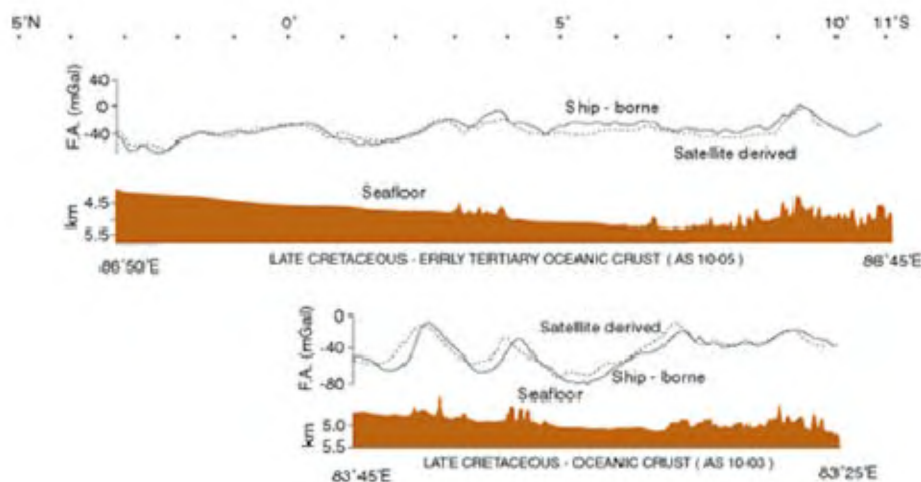


Figure 4. Seafloor topography, ship-borne and satellite-derived free-air gravity anomalies are plotted along the profiles AS 10-03 and 10-05.

deformation at the basement and sediment levels. In contrast, the high in the north between 0.75 and 1.25°N has larger relief at the basement level compared to the overlying sediments. The change in their reliefs perhaps reflects excess deformation of the basement of the northern block. The near-circular shape and amplitude of deformation of block 10 may be explained as pre-existing volcanic construct involved in deformation later. It lies north of the ANS, a large volcanic structure. Considering the trend of deformation similar to others, we believe that the adjoining block 11 in the south is formed during the late Miocene deformation of the crust. The morphological

Miocene deformation of the crust. The morphological expression and variations in the relief at the basement and sediment layer levels of block 10 lead to the pre-existing structure later (to Miocene) deformed. Such an excess basement relief compared to the overlying sediments of the block was also reported on profiles AS 10-03 and 10-05 (ref. 22). The parity in relief points to reactivation/ tectonism of the pre-existing structure.

Details of anticlinal basement structure of the blocks 15 and 19 overlain by about 1.5 km thick sediments noted on the seismic images of the profiles VI58-1, K32-

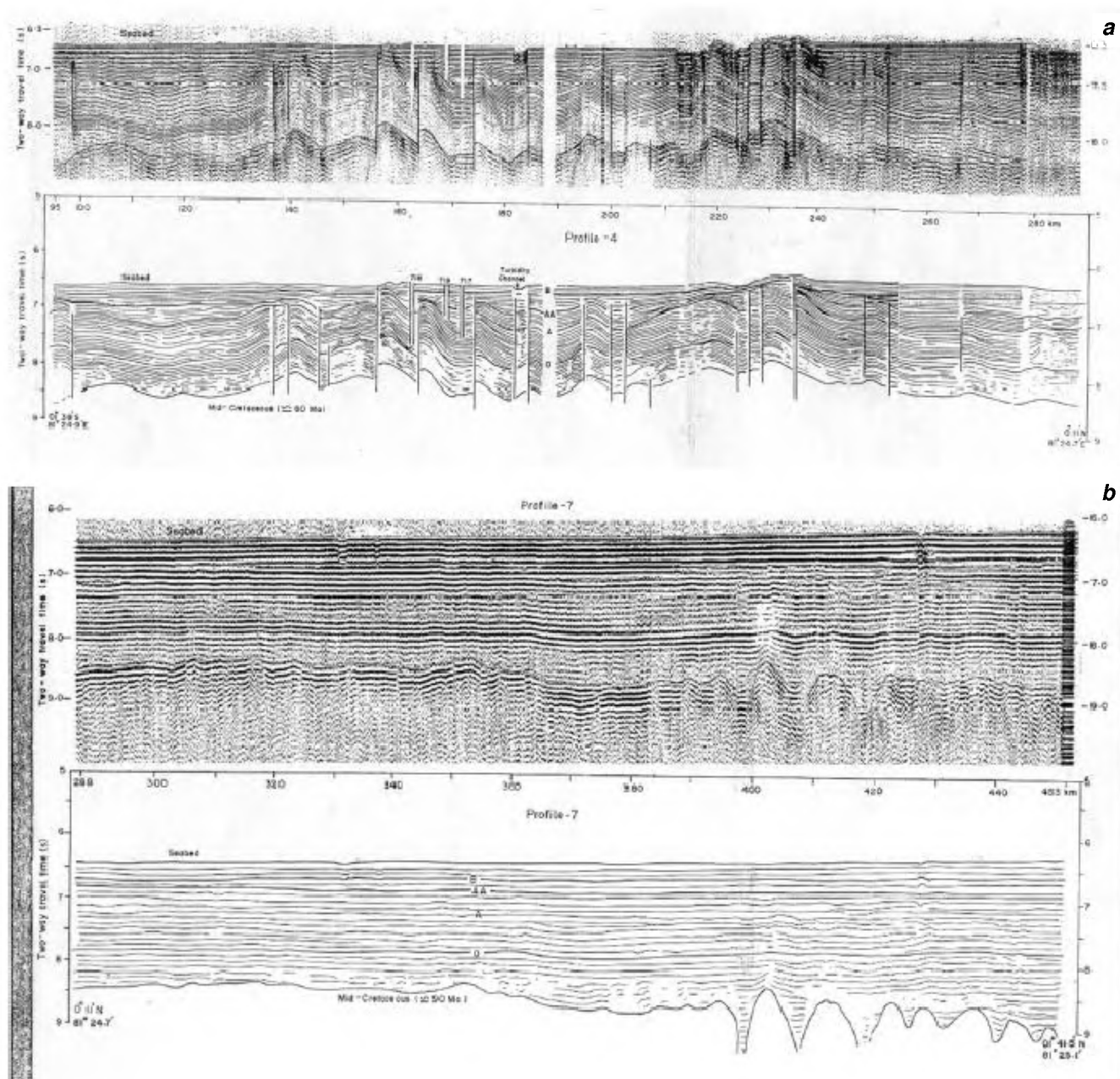


Figure 5. Single-channel seismic reflection records along (a) north-south regional profile 4 covering the deformed blocks 7 and 6 and the trough in between. (b) Profile 7, northern continuation of the profile 4 cover block 22. Line diagrams below show interpreted results. 717–719 are drill sites of ODP Leg 116. Seismic sequence boundaries are denoted by O, A, AA and B.

16 and MK-7 are given in Table 1. They mark low relief and widely spaced faults of the basement. Most of them are bounded by fracture zones. Some of them in the west culminate against the volcanic structure of the seamount. The deformed block 4 (Figure 6 *a*), about 180 km wavelength and about 1.2 km relief in the west is overlain by about 1.0 s thick Miocene to Recent sediments and clearly depicts such changes. Clear offsets between the two blocks, 1 and 2, near Chagos Bank in the west and between 21 and 22 near the Ninetyeast Ridge in the east (Figure 7) are similar to the offsets marked for the deformed blocks of the region. The two deformed blocks in the west near the Chagos Bank and numerous wide deformed blocks in the east near the Ninetyeast Ridge mark a triangular shape to the area of deformation with one vertex in the west and the other two vertices in the east. Thus, they decipher clearly excess crustal deformation in the east.

Correlation between free-air gravity anomaly and seismic structure of the deformed crustal blocks

The deformed crustal blocks that are identified from the available seismic images are correlated with free-air anomalies noted from the ship-borne and satellite gravity anomalies.

Some seismic images of the basement highs and associated gravity signatures were also reported earlier^{5,20} and E-W striking undulations of basement contributing to the observed gravity in the east and the west of Ninetyeast Ridge of the CIOB area were noted^{21,23}. But we have noticed from bathymetric expression, gravity signatures and seismic images, NE-SW trends of the deformed blocks. We, therefore, infer that the gravity highs noted in the study area mark the northeast trending deformed crustal blocks and the near-circular highs of the CIOB correlate with non-deformed basement structural highs related to the ANS, Ninetyeast Ridge and Comorin Ridge (Figure 2). The gravity lows between them mark the basement troughs. Most of them trend NE-SW and the positive free-air gravity anomalies of the CIOB have enabled identification of the deformed crustal blocks and mapping of their mosaic.

Deformation of the crust in the CIOB

A total of 23 such deformed crustal blocks bounded by longitudinal fracture zones 79°E FZ, 80°E FZ, Indira FZ, 84.5°E FZ and 86°E FZ between 77° to 88°E and 5°S to 4°N are noted from the integrated interpretation of the sea-floor topography, gravity and seismic data. They trend mostly NE-SW and NNE-SSW and are associated with

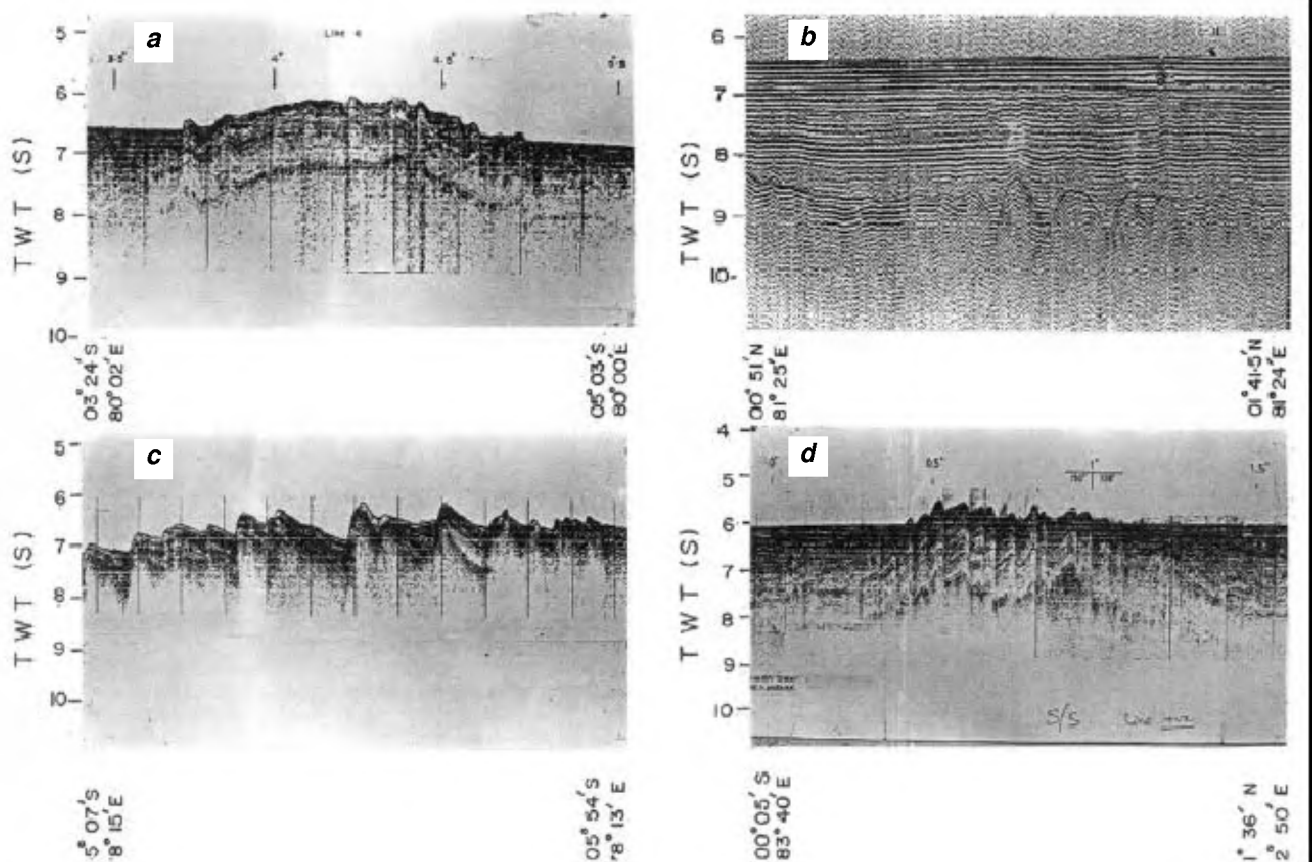


Figure 6 a-d. Seismic reflection records show varied deformed crustal blocks of the CIOB. Locations are shown in Figure 1.

significant free-air gravity (satellite-derived and ship-borne) anomalies, 15 to 60 mGal. They are 100 km long and 60 to 210 km wide, with 0.3 to 2 km relief at the basement level itself and resemble anticlinal structures (Table 1). The anticlinal structures and the volcanic constructs in the west are associated with high-amplitude gravity anomalies (Figure 7; blocks 1 to 14 in Table 1). More number of low-amplitude broad deformed blocks occur to the east of 82°E and they are closely spaced around the ANS. It points to excess convergence of the crust in the region. The causative forces of the deformation are compression, but the reasons for excessive folding and extent in the east are not clearly known. The crust east of 83°E is relatively old and records excessive deformation/shortening; it is anomalous. A late Eocene–early Oligocene plate boundary has been proposed along 86°E FZ¹². The locale is also noted for excess geothermal conditions and seismicity as well (Table 1). If the folding is due to in-plane compressive forces (as suggested) then altered rheology of the rocks forming the crust in the east, being close to plate boundary, became more susceptible to the ridge push forces and is likely to undergo relatively excess deformation. Seismicity has also been noted in the area, which again points to increased stress field causing ex-

cess folding/deformation of the crust. Besides, the voluminous volcanics of the ANS (450 km long, 150 km wide and 3.4 km relief) cause load flexuring/deforming of the lithosphere in the middle of the basin, which has also experienced repeated tectonism/volcanism.

The deformed blocks consist of anticline-like structures and reactivated volcanic constructs (near ANS reflecting the pre-existing deformed crust) involved in the later deformation process of the lithosphere/crust. The offsets between the deformed blocks near the Chagos Bank and the Ninetyeast Ridge indicate crustal shearing and convergence of crust against them in the absence of identified fracture zones marking the deformed process of the crust. The structures near the Ninetyeast Ridge are considerably wide and show that a large area is involved in crustal shearing. From experimental data increasing wavelength of deformation with age of the crust has been proposed⁴. The present study also has revealed increased number of broad low-amplitude deformed crustal features of relatively old crust in the east. Earlier workers have noted from the seismic reflection records of the profiles M31-Vc, M31-2 and V3616 (A) deformed sediments of the fracture zones, especially of the 79°E FZ and 80°E FZ and suggest even the recent ongoing deformation process of Recent times. Thus, the area had experienced periodic deformation²².

Despite the deformation of the crust and NE-SW trends of the deformed blocks, near E-W trends of the magnetic iso-chrons 26 through 34 are remarkable in the CIOB area. We believe that from meagre gravity data several workers^{7,21,23} have inferred E-W trends of the deformed crustal blocks. The magnetic anomalies even show left lateral offset and imply that the older crust in the east, i.e. east of the 82°E FZ adjoins the younger crust of the west¹². Three plate configuration of the Indo-Australian plate comprising Capricorn, Indian and Australian plates and NW-SE compression between Australian and Capricorn plates, and Indian and Australian plates were suggested²⁴. The compression should be northwest following the triangular law of forces of vectors, i.e. parallel to resultant vector and the NE-SW trends of the deformed blocks. Left lateral strike slip motion was also noted across the northern part of the Ninetyeast Ridge^{21,25} and indicated forces in anticlockwise sense in the CIOB area. The strain and stress field within the Indo-Australian plate is mainly contributed by northward-ridge push⁸. Seismicity studies and moment tensor values have revealed near NW-SE compression stress in the area^{25,26}. The Wharton Basin and the Ninetyeast Ridge adjoining the CIOB in the east have recorded NW-SE compression stresses and NE-SW trending gravity highs^{26,27}. Extension, shortening and crustal thickening from west to east have been noted in the area¹⁵. Therefore, E-W trending magnetic isochrons, which are at variance with the seafloor topography, gravity and seismic results need to be investigated in greater detail and close grid deep-tow magnetic studies are needed to

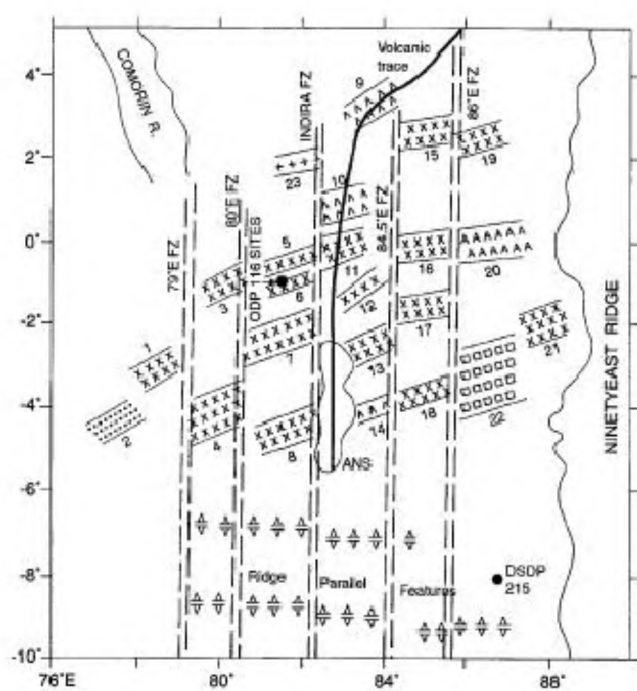


Figure 7. Mosaic map showing NE-SW trending deformed crustal features – areas with dots, crosses, inverted Vs, plus signs, open squares and As are closely spaced high-angle reverse faults (shown in Figure 5 c), anticline basement rises and high-angle faults (shown in Figure 6 a), series of closely spaced high-angle faults and pre-existing basement structures deformed (shown in Figure 6 d), deformed basement overlain by stratified sediments (shown in Figure 6 b), high-angle faults superposed on low-amplitude long wavelength basement rise and abandoned spreading centre respectively. ANS, Afanasy Nikitin seamount.

Table 1. Geophysical signature of deformed crustal blocks of the CIOB area

Deformed block	Satellite free-air gravity anomaly (mGal)		Seismicity in magnitude	Heat flow (mWm ⁻²)	Geometry of deformed block			Sediment thickness (TWT, s)	Time of deformation	Source of data
	Range	Amplitude (approx)			Width (km)	Relief (km)	Fault pattern			
1	- 25 to - 45	20		≈ 140	80	≈ 0.5	Closely spaced high-angle large faults.	0.75	Upper Miocene	Profile C27-07A (ref. 29).
2	- 20 to - 35	15				1.2	Closely spaced high-angle reverse faults.	0.65	Upper Miocene	Profile M31-Vd (ref. 3). Profile C27-07A (ref. 29).
3	- 45 to - 60	20		≈ 57	130-140	0.9	Closely spaced high-angle faults. Anticlinal basement high.	1.64	Upper Miocene	Profile M31-2 or AA' (refs 3 and 23).
4	- 15 to - 55	40			170-180	1.2	Long wavelength anticlinal basement high with high-angle faults with large relief in the north compared to south	1.23	Upper Miocene	Profile M31-2 or AA' (refs 3 and 23) Profile V3616(A) (ref. 32).
5	- 40 to - 60	20			90-100	0.73	Set of high-angle faults.	2.0	Upper Miocene	Profile S22-4 (Present study).
6	- 40 to - 60	20	5.5		50-60	0.6	Set of high-angle faults at regular intervals.	2.0	Upper Miocene	Profile S22-4 (Present study).
7	- 25 to - 55	30		≈ 122	160	2.0	Limited high-angle reverse faults.	1.4	Upper Miocene	Profile V3616(B) (ref. 32). Profile CD-28 (ref. 5). Profile Phedre 81.5° (ref. 33). Profile S22-4 (Present study). Profile C27-06 and V 3305 (ODP Initial Reports, vol. 116).
8	- 15 to - 55	40			150	1.2	Long wave-length low relief basement high with high-angle faults.	1.0	Upper Miocene	Profile CD-28 (ref. 5). Profile V 3616(B) and V3305 (ODP Initial Reports, vol. 116).
9	- 35 to - 55	20			120	0.7	Long wavelength low relief anticlinal structure with limited high-angle faults.	1.5	Upper Miocene	Profile K 32-16 (ref. 34). Profile MK-7. Profile Vi 58-1 (Present study).
10	- 5 to - 45	40			170-180	1.9	Series of closely spaced high-angle faults. Double-peaked high relief anticline (pre-existing structures reactivated).		Upper Miocene	Profiles M 31-3 or BB', S22-11C and S33-11d (ref. 20). Profile S22-9 (Present study).
11	+ 10 to - 50	60		72-112	180-220	2.0	Basement high (large relief), anticline associated with a set of high-angle faults (perhaps pre-existing structure).		Upper Miocene	Profiles M31-3, S22-1a and S22-11b (ref. 20). Profile V 29-01 (ODP Initial Reports, vol. 116).
12	- 55 to - 40	15			120	0.8	Low relief basement high, anticline associated with few minor faults.	1.6	Upper Miocene	(Ref. 32).
13	- 10 to - 50	40		70-76		1.3	Basement high with steep northern flank associated with limited high-angle faults.	1.0	Upper Miocene	Profile AS10-03 (ref. 22). Profile MK-7 (ref. 20).
14	- 15 to - 50	35			200-210	2.0	Limited high-angle faults. Pre-existing structure reactivated.	0.25	Upper Miocene	Profile AS10-03 (ref. 22).
15	- 15 to - 30	15			50-60	0.4	Low relief basement high with closely spaced high-angle faults.	0.6		Profile K32-16 (ref. 34) Profile Vi 58-1(Present study).
16*	- 25 to - 45	20		≈ 62						
17*	- 30 to - 45	15								
18*	- 25 to - 50	25	5.0	≈ 78						
19	0 to - 40	40	7.0		50-60	0.3	Limited faults and gradual deepening of basement high in the west.	0.8	Upper Miocene (?)	Profile Vi 58-1 (Present study).
20	- 15 to - 35	20			130-140	0.8	Limited high-angle basement faults and pre-existing structure.	1.0	Upper Miocene	Profile -10-05 (ref. 22).
21	+ 20 to - 45	65	6.5							
22	- 5 to - 45	30		≈ 82	330	1.0	Long wavelength basement high with closely spaced high-angle faults.	0.4	Upper Miocene	Profile -10-05 (ref. 22).
23	- 55 to - 70	15		≈ 100	150-180	1.0	Series of low relief short wavelength basement highs with limited or no faults.	2.0	Pre-Upper Miocene	Profile S22-7 (Present study). Profile S22-8 (Present study). Profile C1708 (ODP Initial Reports, vol. 116).

*Anticlines inferred from positive gravity closures.

confirm the trends of the iso-chrons. Thus, we suggest age-related latitudinal variation in convergence and less mechanical strength of the rocks in the east, effective NW-SE compression and NE-SW and/or NNE-SSW deformed crustal blocks. The relatively high pressure and temperature conditions at the palaeo plate boundary near 86°E, pre-existing large volcanic construct in the centre of the unified Indo-Australian plate and later igneous intrusions of the ANS effectively altered the physical state of the crust/lithosphere and made it conducive for localization of deformation. The altered rheology of the rocks forming the crust of the CIOB became susceptible to the compressive forces and locale for the deformation after completion of the suturing process of the Indo-Eurasian plates and formation of the Himalayas in the north.

The extent of the intense deformed crust, locale of the NE-SW trending deformed structures and spatial variations in the deformation style are identified more precisely from the free-air gravity confirmed by the seismic images. The order of deformation/dislocation of the crust is consistently reflected in gravity anomaly amplitudes as well. They could be distinguished, from the identified anomalies of a chain of volcanic constructs that are parallel to 82.5°E longitude in the middle of the CIOB, as emplaced by the Kerguelen mantle plume in the east between 88° and 90°E, and of spreading ridge processes in the south, south of 6°S. A large number of earthquake epicentres of medium (3.5 to 6.0) and large (above 6.0) magnitude also occur close to few of the structures and reveal the continued stress regime in the area as well. Thus, the asymmetric NE-SW trending upthrust 65–78 Ma oceanic crust blocks arise most likely from plate-boundary forces and anticlockwise rotation and compressive forces.

Summary

Intense deformation of the late Cretaceous–early Tertiary oceanic crust of the CIOB has been noted between latitudes 5°S to 4°N and longitudes 77° and 88°E. It comprises 23 NE-SW trending upthrust crustal blocks (anticlines like deformed basement structures and reactivated pre-existing structures) well reflected in satellite free-air gravity anomalies data and confirmed by geomorphology and seismic images. The positive and negative anomaly closures enable us to mark upthrust/volcanic and trough-like structures of the basement respectively. The larger number of deformed crustal blocks of the mosaic map in the east marks intense deformation leading to increased longitudinal variation in shortening. The study also distinguishes the various types of crustal features and their nature of deformation at the basement and their reflections in the gravity and seismic data.

The NW-SE to NNW-SSE compression leads to the deformation and formation of the NE-SW deformed upthrust crustal blocks. Identification of volcanic constructs

and their trace in the middle of the basin, parallel to 88°E longitude in the east, northwest and in the south enable to distinguish the deformed crustal blocks and the volcanic constructs and their good correlations with the geophysical signatures. A total mosaic map of the deformed crustal blocks of the basin and the volcanic constructs has been prepared.

The altered rheology due to changed physical state of the rocks forming the crust/lithosphere in the mid-plate position and due to excess volcanic load had accentuated and contributed to the periodic deformation of the weak crust. The lithosphere of the locale is affected by the excess volcanic constructs and *P–T* conditions.

1. Louden, K. E., Variations in crustal structure related to intraplate deformation: evidence from seismic refraction and gravity profiles in the Central Indian Basin. *Geophys. J. Int.*, 1995, **120**, 375–392.
2. Cochran, J. R. *et al.*, Shipboard Scientific Party, ODP Leg 116 site survey. Proceedings ODP Init. Reports, 116, College Station, TX (Ocean Drilling Program), 1987, pp. 197–210.
3. Levchenko, O. V. and Merklin, L. R., The M31 cruise seismic reflection studies. In *Intraplate Deformation of the Central Indian Ocean Basin* (eds Neprochnov, Yu. P. *et al.*), Geol. Soc. India, Mem. 39, 1998, pp. 95–102.
4. Bull, J. M. and Scrutton, R. A., Seismic reflection images of intraplate deformation, Central Indian Ocean, and their tectonic significance. *J. Geol. Soc. London*, 1992, **149**, 955–966.
5. Bull, J. M., Structural style of intraplate deformation, Central Indian Ocean Basin: evidence for the role of fracture zones. *Tectonophysics*, 1990, **184**, 213–228.
6. Cochran, J. R. *et al.*, Himalayan uplift, sea level, and the record of Bengal Fan sedimentation at the ODP Leg 116 Sites. Proc. ODP, Sci. Results, 116, College Station, TX (Ocean Drilling Program), 1990, pp. 397–414.
7. Weissel, J. K., Anderson, R. N. and Geller, C. A., Deformation of the Indo-Australian plate. *Nature*, 1980, **287**, 284–291.
8. Evsykov, Yu. D., Subrahmanyam, C., Murthy, K. S. R. and Rai, S. N., Bathymetric investigations in the S22 cruise area. In *Intraplate Deformation of the Central Indian Ocean Basin* (eds Neprochnov, Yu. P. *et al.*), Geol. Soc. India, Mem. 39, 1998, pp. 29–37.
9. Curray, J. R. and Munasinghe, T., Timing of intraplate deformation, northeastern Indian Ocean. *Earth Planet. Sci. Lett.*, 1989, **94**, 71–77.
10. Gopala Rao, D., Krishna, K. S. and Sar, D., Crustal evolution and sedimentation history of the Bay of Bengal since the Cretaceous. *J. Geophys. Res.*, 1997, **102**, 17747–17768.
11. Krishna, K. S., Bull, J. M. and Scrutton, R. A., Evidence for multi-phase folding of the central Indian Ocean lithosphere. *Geology*, 2002, 8–12.
12. Krishna, K. S. *et al.*, Tectonic model for the evolution of oceanic crust in the northeastern Indian Ocean from the Late Cretaceous to the Early Tertiary. *J. Geophys. Res.*, 1995, **100**, 20,011–20,024.
13. Gordon, R. G., The plate tectonic approximation: plate nonrigidity diffuse plate boundaries and global plate reconstructions. *Annu. Rev. Earth Planet. Sci.*, 1998, **26**, 615–642.
14. Bull, J. M. and Scrutton, R. A., Fault reactivation in the Central Indian Ocean and the rheology of oceanic lithosphere. *Nature*, 1990, **344**, 855–858.
15. Montesi, L. G. J. and Zuber, M. T., Spacing of faults at the scale of the lithosphere and localization instability: 2 Application to the Central Indian Basin. *J. Geophys. Res.*, 2003, **108**, 2111, DOI: 10.1029/2002JB001924.

16. Montesi, L. G. J. and Zuber, M. T., A unified description of localization for application to large-scale tectonics. *J. Geophys. Res.*, 2002, **107**, 10, 1029/2001JB000465.
17. Sandwell, D. T. and Smith, W. H. F., Marine gravity anomaly from Geosat and ERS1 satellite altimetry. *J. Geophys. Res.*, 1997, **102**, 10, 039–10,054.
18. Buryanov, V. B., Milanovsky, A. A. and Rusakov, O. M., The S22 cruise gravity investigations, In *Intraplate Deformation of the Central Indian Ocean Basin* (eds Neprochnov, Yu. P. *et al.*) Geol. Soc. India, Mem. 39, 1998, pp. 54–61.
19. Verbysky, E. V. and Lobkovsky, L. I., On the mechanism of heating up of the Indo-Australian plate. *J. Geodyn.*, 1993, **17**, 27–38.
20. Neprochnov, Yu. P., Gopala Rao, D., Subrahmanyam, C. and Murthy, K. S. R., Intraplate deformation of the Central Indian Ocean Basin. Geol. Soc. India, Mem. 39, 1998, pp. 1–250.
21. Stein, S. and Okal, E. A., Seismicity and tectonics of the Ninety-east Ridge area: Evidence for internal deformation of the Indian plate. *J. Geophys. Res.*, 1978, **83**, 2233–2246.
22. Krishna, K. S., Ramana, M. V., Gopala Rao, D., Murthy, K. S. R., Malleswara Rao, M. M., Subrahmanyam, V. and Sarma, K. V. L. N. S., Periodic deformation of oceanic crust in the Central Indian Ocean. *J. Geophys. Res.*, 1998, **103**, 17, 859–17,875.
23. Neprochnov, Yu. P., Levchenko, O. V., Gopala Rao, D., Subrahmanyam, C. and Murthy, K. S. R., Correlation of intraplate deformation structures and geophysical field anomalies. In *Intraplate Deformation of the Central Indian Ocean Basin* (eds Neprochnov, Yu. P. *et al.*), Geol. Soc. India, Mem. 39, 1998, pp. 222–228.
24. Royer, J.-Y. and Gordon, R. G., The motion and boundary between the Capricorn and Australian plates. *Science*, 1997, **277**, 1268–1274.
25. Singh, D. D., Strain deformation in the northern Indian Ocean. *Mar. Geol.*, 1988, **79**, 105–118.
26. Stein, C. A., Cloetingh, S. and Wortel, R., Sea-sat derived gravity constraints on stress and deformation in the northeast Indian Ocean. *Geophys. Res. Lett.*, 1989, **16**, 823–828.
27. Petroy, D. E. and Wiens, D. A., Historical seismicity and implications for diffuse plate convergence in the northeast Indian Ocean. *J. Geophys. Res.*, 1989, **94**, 12, 301–12,319.
28. Fisher, R. L., Jantsch, M. J. and Comer, R. L., General bathymetric chart of the Oceans (GEBCO), Canadian Hydrographic Service, Ottawa, Canada, 1982.
29. Orman, J. V., Cochran, J. R., Weissel, J. K. and Jestin, F., Distribution of shortening between the Indian and Australian plates in the central Indian Ocean. *Earth Planet. Sci. Lett.*, 1995, **133**, 35–46.
30. Levchenko, O. V., Tectonic aspects of intraplate seismicity in the northeastern Indian Ocean. *Tectonophysics*, 1989, **170**, 125–139.
31. Cloetingh, S. and Wortel, R., Stress in the Indo-Australian Plate. *Tectonophysics*, 1986, **132**, 49–67.
32. Geller, C. A., Weissel, J. K. and Anderson, R. N., Heat transfer and intraplate deformation in the Central Indian Ocean. *J. Geophys. Res.*, 1983, **88**, 1018–1032.
33. Chamot-Rooke, N., Jestin, F., de Voogd, B. and Phedre Working Group, Intraplate shortening in the central Indian Ocean determined from a 2100-km-long north-south deep seismic reflection profile. *Geology*, 1993, **21**, 1043–1046.
34. Milanovsky, V. E., Levchenko, O. V. and Merklin, L. R., Some seismic data in the Red Sea and Indian Ocean. In *General Study of Oil and Gas Potential in the Indian Ocean*, Nauka, Moscow, 1982, pp. 140–156 (in Russian).

ACKNOWLEDGEMENTS. We are grateful to V. K. Gaur and the late A. L. Yanshin, Area Coordinators of ILTP project B-2.14 for their guidance. DST, India and the RAS, Russia supported the project. CSIR Emeritus scheme has provided financial grant to Gopala Rao. Thanks are also due to E. Desa, Director NIO, Goa for encouragement. This is NIO contribution number 3857.

Received 15 April 2003; revised accepted 16 November 2003